CHARACTERISTICS OF UNDULAR HYDRAULIC JUMPS: EXPERIMENTAL APPARATUS AND FLOW PATTERNS

By H. Chanson[1] and J. S. Montes[2]

ABSTRACT: In open channels, the transition from supercritical to subcritical flows is called a hydraulic jump. For low upstream Froude numbers, free-surface undulations develop downstream of the jump and the hydraulic jump is called an undular jump. New experiments on undular hydraulic jumps were performed in a rectangular channel in which the upstream flows were fully developed turbulent shear flows. In this paper, the main flow patterns are described. Visual and photographic observations indicate five types of undular jumps. One of the main flow characteristics is the presence of lateral shock waves for Froude numbers larger than 1.2. The results show that the disappearance of undular jump occurs for Froude numbers ranging from 1.5 to 2.9, and the wavelength and amplitude of free-surface undulations are functions of the upstream Froude number and the aspect ratio y_c/W.

INTRODUCTION

In open channel flow, the transition from a rapid to tranquil flow is called a hydraulic jump. It is characterized by the development of large-scale turbulence, surface waves, energy dissipation, and air entrainment. The flow conditions downstream of the jump are deduced from the momentum and continuity equations and the upstream flow conditions. For a horizontal rectangular channel of constant channel width, and neglecting the bed and wall friction, it can be shown that [Streeter and Wylie (1981)]

$$\frac{h_2}{h_1} = \frac{1}{2}\left(\sqrt{1 + 8\,F_1^2} - 1\right); \quad \frac{F_2}{F_1} = \frac{2^{3/2}}{\left(\sqrt{1 + 8\,F_1^2} - 1\right)^{3/2}} \tag{1, 2}$$

where the subscripts 1 and 2 = upstream and downstream flow conditions of the hydraulic jump (Fig. 1), respectively; and F = Froude number.

The energy dissipation within a hydraulic jump can be derived from the energy equation using the results [(1) and (2)]

$$\frac{\Delta H}{y_c} = \frac{(h_2 - h_1)^3}{4h_1h_2y_c} \tag{3}$$

where ΔH = head loss; and y_c = critical depth.

A hydraulic jump of low height is characterized by free-surface undulations downstream of the jump (Fig. 2), and is called an undular jump (in Fig. 2 the flow goes from right to left). For an undular jump, the energy loss [(3)] is very small but not zero. As the undular jump does not have a marked roller, the energy losses are radiated forward in a train of stationary waves (Montes 1979, 1986). The undulations extend far downstream of the jump with decaying wave lengths, and can occupy a significant length of the channel.

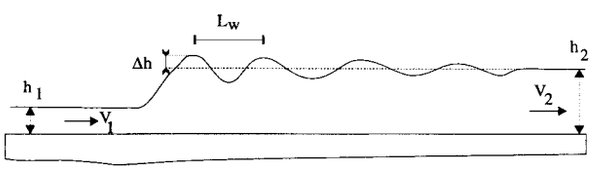

FIG. 1. Undular Hydraulic Jump

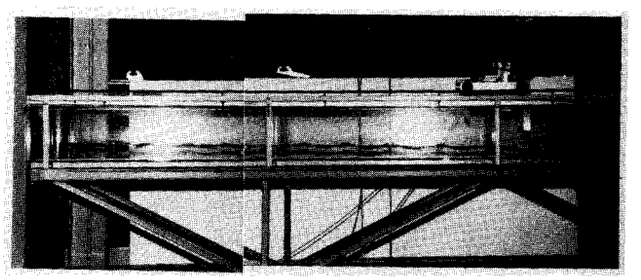

FIG. 2. Experiment — y_c/W = 0.138, F_1 = 1.62, W = 0.25 m (UJ Type C)

[1]Lect., Hydr. and Fluid Mech., Dept. of Civ. Engrg., Univ. of Queensland, Brisbane QLD 4072, Australia.
[2]Sr. Lect., Dept. of Civ. and Mech. Engrg., Univ. of Tasmania, Hobart TAS 7000, Australia.

Note. Discussion open until July 1, 1995. To extend the closing date one month, a written request must be filed with the ASCE Manager of Journals. The manuscript for this paper was submitted for review and possible publication on February 14, 1994. This paper is part of the ***Journal of Hydraulic Engineering***, Vol. 121, No. 2, February, 1995. ©ASCE, ISSN 0733-9429/95/0002-0129–0144/$2.00 + $.25 per page. Paper No. 7859.

Bibliographic Review

Most hydraulic and fluid mechanics textbooks ignore the case of undular hydraulic jumps in their section on open channel flows. Some specialized textbooks (Rouse 1938; Chow 1959; Henderson 1966) indicate the occurrence of an undular jump for $F_1 < 1.7$, but do not detail its flow properties.

Some experimental studies of hydraulic jumps include some undular jump cases; for e.g., Bakhmeteff and Matzke (1936), Binnie and Orkney (1955), and Sandover and Holmes (1962). However, these researchers did not detail the specific properties of undular jumps. Other researchers particularly studied undular jumps for e.g., Lemoine (1948), Serre (1953), Iwasa (1955), Jones (1964), and Andersen (1978). But all these analyses were based on an analogy with an undular surge advancing in still water, and the various results are sometimes conflicting.

Montes (1979) showed that the analogy between undular jump and undular surge does not take into account flow characteristics. In the case of undular jumps, turbulent boundary layers are partially or fully developed along both the channel bed and the sidewalls. Further, as the jump extends over a great length, the assumption of negligible bottom and sidewall friction (used in undular surge calculations) is unrealistic.

Fawer (1937) performed an interesting study but his work was ignored by most researchers. This is despite Fawer's clearly detailing the main features of undular hydraulic jumps.

Montes (1986) and Ryabenko (1990) presented two pertinent and independent studies. Their results refuted the principle of an analogy between undular jump and undular surge. Further, they suggested that the transition between an undular jump and a weak jump may occur for upstream Froude numbers in the range 1.0 to 3.6, the transition being a function of the upstream flow conditions.

Undular Jump Flow Situations

An undular hydraulic jump may occur in irrigation and water supply channels, in estuaries during some period of the tides, and in narrow or shallow straights subjected to strong currents.

When an undular jump takes place in a channel, waves of large amplitudes develop and propagate downstream of the jump. These undulations may overtop and damage the channel banks extensively. The propagation of free-surface waves downstream of undular jumps must be taken into account for the design of canals and the maintenance of natural channels. For natural channels and canals, the embankment height must be higher than the crest of the free-surface undulations to prevent erosion and ultimately the destruction of the banks. Further, the propagation of free-surface waves might impose additional impact loads, perturbations, and vibrations on downstream structures (e.g., gates, locks, or weirs). Chandran and Venkatraman (1985) described the case of an undular jump immediately upstream of pump intakes. Induced by the jump, the waves perturbed the pump operation; thus, the channel was modified to avoid the undular hydraulic jump. Also, the propagation of downstream waves over long distances might affect or prevent navigation in the channel.

Undular hydraulic jumps may also occur aft of ships traveling in canals and shallow waters. Haslewood (1985) presented a comprehensive study of the problem. The appearance of undular jumps coincides with a rapid increase in ship resistance in canals or shallow waters. The growth in ship resistance is attributed to the onset of critical conditions alongside the ship and the sudden apparition of undular jump waves aft of the ship.

New experimental data relating to free-surface undulations downstream of an undular jump are presented here (Table 1). The experiments were performed in a rectangular channel with fully developed upstream shear flow conditions. The results are compared with existing data, and the effects of channel width and bottom shear stress are discussed. Full details of the experimental data are given by Chanson (1993).

EXPERIMENTAL APPARATUS

Experiments were performed in a 20-m-long channel of a uniform rectangular section made of glass (bottom and sidewalls), located in the Hydraulic Laboratory of the University of Queensland (Fig. 2). The channel width is 0.25 m and the sidewall height is approximately 0.27 m. It is supported on an elevated steel truss that spans the main supports. The channel slope can be adjusted using a geared lifting mechanism.

Regulated flows are supplied from a constant head tank feeding an inlet transition to the channel via a butterfly valve mounted on the head tank discharge line. Tailwater levels are controlled by a radial gate fitted at the downstream channel end. The upstream face of the gate is covered by a dozen layers of 75% shade cloth to prevent wave reflection from the gate. Further details on the channel were given by Isaacs and Macintosh (1988).

In this study, the water discharge ranges from 2 to 30 L/s, the upstream Froude number is between 1.05 and 3.0, the aspect ratio y_c/W is in the range 0.075 to 0.455, and the channel slope ranges from 0.2° to 4.5°.

TABLE 1. Summary of Experimental Flow Conditions

Reference (1)	q_w (m^2/s) (2)	h_1 (m) (3)	F_1 (4)	y_c/W (5)	U/S (Flow)[a] (6)	Number of experiments (7)	Comments (8)
Present study, University of Queensland	0.008	0.010–0.017	1.13–2.6	0.075	F/D[b]	6	Series HMUP1 W = 0.25 m
	0.020	0.016–0.032	1.14–2.91	0.137	F/D[b]	18	Series HMUP2
	0.028	0.029–0.041	1.08–1.79	0.172	F/D[b]	8	Series HC3
	0.040	0.027–0.051	1.11–2.83	0.219	F/D[b]	19	Series HMUP3
	0.042	0.037–0.051	1.10–1.77	0.224	F/D[b]	9	Series HC1
	0.062	0.061	1.31	0.292	F/D[b]	1	Series HC0
	0.08	0.067–0.084	1.05–1.49	0.347	F/D[b]	7	Series HC4
	0.12	0.091–0.109	1.07–1.40	0.454	F/D[b]	6	Series HC2
University of Tasmania	—	—	1.1–10	—	P/D[c]	—	W = 0.4 m
Andersen (1978)	0.066	0.067	1.22	N/A[d]	N/A	1	—
Bakhmeteff and Matzke (1936)	0.327	0.135–0.155	1.75–2.1	1.45	P/D[c]	3	W = 0.152 m
Fawer (1937)	0.02–0.07	0.02–0.08	1.3–1.75	0.11–0.27	P/D[c]	5	W = 0.303 m
Binnie and Orkney (1955)	0.069–0.084	0.064	1.12–1.52	N/A[d]	P/D[c]	6	—
Darcy and Bazin (1865)	1.55(?)	0.43	1.76(?)	N/A[d]	F/D[c]	1	Aqueduc of Crau, canal of Craponne (France).
Hager and Hutter (1984)	0.0987	0.081	1.37	0.332	P/D[c]	1	W = 0.3 m, α = 0.08 degree
Iwasa (1955)	N/A[d]	N/A[d]	1.29–4.14	N/A[d]	N/A[d]	34	—
Montes (1979)	N/A[d]	N/A[d]	1.25–2	N/A[d]	P/D[c]	8	W = 0.2 m
Yasuda et al. (1993)	0.025–0.085	0.023–0.067	1.5–2.17	0.101–0.208	F/D[b] and P/D[c]	4	W = 0.3–0.4 m horizontal channel
Ryabenko (1990)	0.025–0.38	0.03–0.2	1–4.0	0.04–0.25	F/D[b] and P/D[c]	13	W = 1 m

[a]Upstream flow conditions.
[b]Fully developed boundary layer flow (i.e., $\delta = h_1$).
[c]Partially developed boundary layer flow (i.e., $\delta/h_1 < 1$).
[d]Not available.

Instrumentation

The water discharge is measured typically with a bend meter installed in the discharge line from the constant head tank. For small discharges (i.e., $Q_w < 10$ L/s), the discharge can be measured using a calibrated 300-L tank. The percentage error is expected to be less than 5%.

Longitudinal flow depths are measured using a rail-mounted pointer gauge positioned over the channel's centerline. The gauge is accurate within 0.5 mm. The flow depth measurements were the mean value over a period of 1 min. The distance along the flume from the channel entrance is measured with a meter line; the error being less than 0.5 cm. The wave lengths and wave amplitudes were deduced from the free-surface profile measurements. Photographs were taken during the experiments and were used to check the visual observations of the locations of the lateral shock waves, wave crests, and wave bottoms.

The velocity, pressure, and specific energy measurements were performed using a Pitot tube. The Pitot tube has an external diameter Ø = 3.3 mm and the pressure head at the tip is measured through a 1 mm diameter hole. The distance between the tip of the probe and the lateral pressure points (Ø = 0.5 mm) is 20 mm. During the experiments, the Pitot tube was connected to a 30° inclined manometer by two 2-m-long hard nylon tubes (Nylex: outside Ø = 6.35 mm, inside Ø = 4.32 mm). The manometer consists of two identical glass tubes open to the atmosphere at the top end, and was fixed at the same location for all measurements. The first pressure reading gives the total head and the one indicates the pressure head plus the elevation.

The translation of the Pitot tube in the direction perpendicular to the channel bottom is controlled by a fine adjustment traveling mechanism connected to a Mitutoyd digimatic scale unit. The error in the vertical position of the Pitot tube is less than 0.1 mm. The longitudinal translation of the Pitot tube is controlled manually; the Pitot tube and the digimatic scale unit are fixed to an L-shaped aluminum beam clamped to the channel top. The error in the longitudinal location of the Pitot tube is less than 5 mm.

At a given cross section and at a distance y from the channel bed, the local total head H, pressure P, velocity V, and specific energy E can be deduced from the two manometer readings, the channel slope, and the bed elevation.

Preparation of Experiments

During the experiments, the location of the hydraulic jump was controlled by the downstream gate, channel slope, and discharge. The channel slope and the discharge control the quasi-uniform flow upstream of the jump, and the downstream gate acts as a downstream control.

Repetitions of the same experiments, over several different days, indicated that the location of the start of the undular jump could be controlled to within about ± 10 mm.

For all the experiments, the start of the undular jump was located at a distance from the channel entrance of between 9.5 and 15 m. For the upstream flows, the boundary layer was fully developed and the boundary layer thickness was equal to the flow depth.

Upstream Flow Conditions

The main upstream flow characteristics were investigated 10.9 m downstream of the channel entrance for discharges ranging from 2 to 30 L/s and Froude numbers between 1.1 and 2.4. During the experiments, the friction factor was deduced from uniform flow measurements performed in the channel before undular jump was established. For the present series of experiments, the friction factor f ranges from 0.015 to 0.026. These values correspond to an equivalent surface roughness k_s, between 0.01–0.15 mm. For the same channel, Isaacs and Macintosh (1988) deduced k_s = 0.05 mm for a water discharge Q_w = 20 L/s and a slope of 0.11°.

For all the experiments, the upstream centerline velocity distributions show that the bottom turbulent boundary layer reached the free surface upstream of the measurement location. Typical examples are shown in Fig. 3. The data clearly shows the boundary layer was fully developed for all investigated flow conditions. At the measurement location (i.e., x = 10.9 m), the velocity distribution can be approximated by a power law

$$\frac{V}{V_{max}} = \left(\frac{y}{h}\right)^{1/N} \tag{4}$$

where V_{max} = maximum velocity at the free surface (on the centerline); y = distance measured perpendicular to the channel bottom; and h = flow depth. The results [Chanson (1993)] indicate that the exponent N ranges from 6.9 to 8.8. For uniform flows, Chen (1990) derived a theoretical relationship between the exponent N of the power law velocity distribution, and the friction factor f as

$$N = K\sqrt{\frac{8}{f}} \tag{5}$$

where K = Von Karman constant (K = 0.4). A comparison shows a good agreement between the values of N deduced from the data and the predictions of [(5)].

A detailed analysis of the upstream flow conditions indicates that the ratio of the mean velocity on the centerline $(V_m)_{CL}$ to the mean flow velocity $Q_w/(W\,h)$ ranges from 1.05 to 1.35, where W is the channel width. These values suggest that the three-dimensional effects of the lateral boundary layers on the sidewalls are not negligible.

The analysis of the pressure distributions at x = 10.9 m clearly shows the centerline pressure distribution upstream of an undular jump is perfectly hydrostatic.

CHARACTERISTIC FLOW PATTERNS

Classification of Undular Jumps

Visual and photographic observations indicate the following five types of undular jumps (Fig. 4):

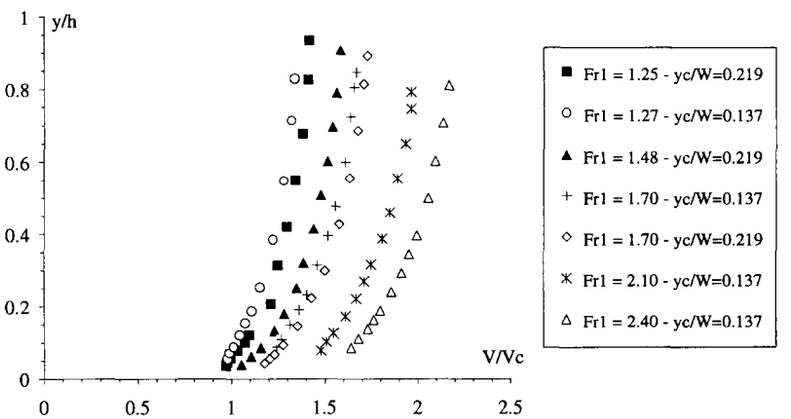

FIG. 3. Typical Velocity Distributions Upstream of Undular Jump

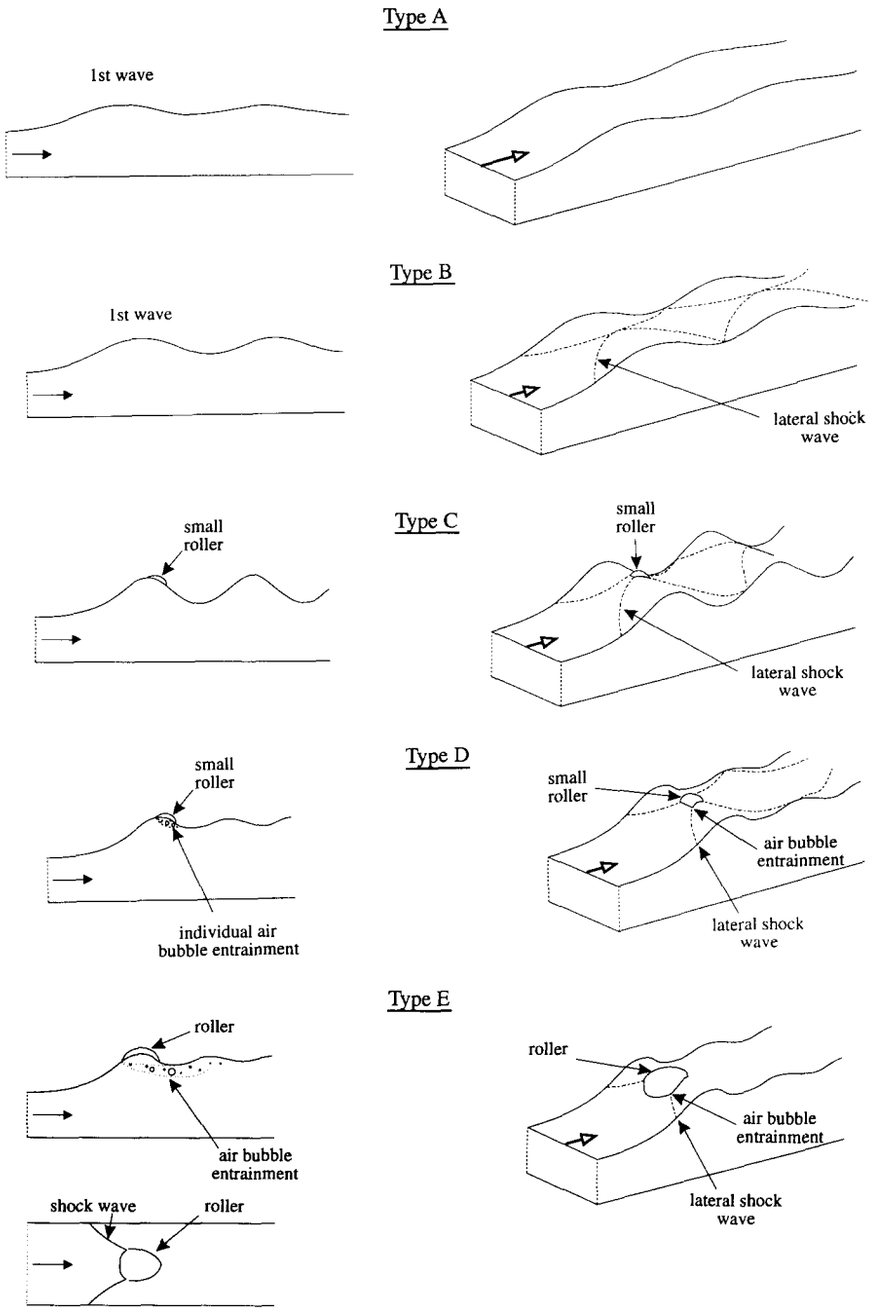

FIG. 4. Classification of Undular Hydraulic Jumps

1. Type A: $1 \leq F_1 \leq F^A$
   For Froude numbers slightly above unity, free-surface undulations of small amplitude and relatively long wavelength develop. The flow is two-dimensional. No roller or shock waves are visible.
2. Type B: $F^A \leq F_1 \leq F^B$
   With an increase of the upstream Froude number, lateral shock waves start to develop upstream of the first wave crest. The shock waves intersect slightly downstream of the top of the first wave. After intersecting, the shock waves continue to propagate and reach the opposite sidewall almost at the location of the wave bottom. The waves are reflected and intersect around the top of the second wave. Viewed from above, the flow downstream of the first wave crest looks like a succession of lozenges aligned along the channel centerline.
3. Type C: $F^B \leq F_1 \leq F^C$
   For larger Froude numbers, the lateral shock waves intersect at the top of the first wave. At this first intersection, a wave-breaking mechanism develops, a small roller appearing

on the top of the first wave, immediately downstream of the intersection of the shock waves. The roller has a cockscomb shape and is located on the jump centerline. It is small compared to the wave (Fig. 4). Such a roller is not observed on the second and subsequent waves.

4. Type D: $F^C \leq F_1 \leq F^D$
   At higher Froude numbers, the undular jump features lateral shock waves, a roller, and individual air bubble entrainment at the top of the first wave (Fig. 4). The bubbles are entrapped at the intersection of the lateral shock waves and the roller, and are entrained over a short distance (less than a single wavelength). A smaller roller might appear at the top of the second wave but no air bubble entrainment is observed there.
5. Type E: $F^D \leq F_1 \leq F^E$
   Just before the disappearance of free-surface undulations downstream of the jump, the roller at the top of the first wave becomes larger and wider. The roller is (blocked) bounded laterally by the lateral shock waves. A top view of the first wave crest shows a characteristic W shape formed by the roller on the centerline and the lateral crosswaves (Fig. 4). The width of the roller remains smaller than the channel width. A nonnegligible air bubble entrainment is observed. The air bubbles can be entrained as far as the second crest.

For upstream Froude numbers larger than the critical value F^E, the free-surface undulations downstream of the jump disappear. The jump becomes a weak hydraulic jump and the roller is fully developed over the entire channel width. In the present study, the disappearance of the undular jump is defined by the disappearance of the second and subsequent wavelengths; i.e., when no energy is radiated forward in a train of stationary waves. It must be emphasized that even a weak jump might show an initial undulation immediately downstream of the roller. However, no subsequent undulations are observed with a weak jump.

For the undular jump types C, D, and E, visual observations indicate that the lateral shock waves intersect on the first crest. Subsequent cross-wave intersections do not occur on the wave crests; the length of the shock waves becomes longer than the wavelength of free-surface crests. With increasing Froude numbers, both the wavelength and shock wavelength decrease. But the rate of decrease of the wavelength is larger than that of the cross-wave length.

The observations obtained during the experiments are summarized in Table 2. The transition Froude numbers F^A, F^B, F^C, F^D, and F^E are presented as a function of the aspect ratio y_c/W in Fig. 5. Previous experimental works are also summarized in Table 2.

The present classification applies to undular jumps with upstream, fully developed shear flows. Ryabenko (1990) performed experiments with nonhydrostatic pressure distributions upstream of the jump and proposed another classification. Ryabenko's work suggests that, for upstream flow conditions with nonhydrostatic pressure distribution, the free-surface undulations disappear at lower Froude numbers than for an upstream hydrostatic pressure distribution. Henderson (1966) discussed the role of bottom roughness. His photographs suggest the transition from undular to weak jump occurs at larger Froude numbers for a rough bed than for a smooth bed.

Longitudinal Flow Pattern

For upstream Froude numbers near unity, the flow pattern downstream of the first crest is two dimensional (undular jump type A) or symmetrical around the centerline (undular jump type B) down to the downstream gate.

For undular jumps of types C, D, and E (i.e., $F_1 > F^B$), a different free-surface pattern is observed (Fig. 6). Immediately downstream of the first crest, the free surface shows a steady, organized, and symmetrical flow pattern. Each wave is clearly marked and maximum wave height is located on the centerline. At the bottom of each wave, the lowest free-surface point is on the centerline. The free surface along the sidewalls follows the centerline flow pattern (with the same wavelength and phase shift), but with much smaller amplitudes. Darcy and Bazin (1865), Fawer (1937), and Hager and Hutter (1984) also observed similar patterns. For the experiments of Fawer (1937) and Hager and Hutter (1984), the channel width was 0.303 m and 0.30 m, respectively.

Downstream of the organized flow region, the free surface develops a chaotic, unsymmetric, unsteady three-dimensional pattern. The wave motion for this disorganized flow pattern shows no visible periodicity in any direction. The free surface at the sidewalls is subject to large unsteady fluctuations. Some experimental data reported by Darcy and Bazin (1865, Fig. 20) showed the same phenomenon.

Further downstream, a damping flow region exists. The wave amplitudes at the free surface are damped rapidly over the entire width of the channel, and the free surface becomes almost quiescent.

Visual observations indicate the length of the organized flow region decreases with an in-

TABLE 2. Characteristic Froude Numbers

Reference (1)	y_c/W (2)	F^A (3)	F^B (4)	F^m (5)	F^C (6)	F^D (7)	F^E (8)	Remarks (9)
Present work	0.075	1.22	1.72		2.10	2.40	>2.6	Series HMUP1
	0.137	1.22	1.68	1.68	1.80	2.4	2.91	Series HMUP2
	0.172	1.2	1.45	1.58	1.7	—	—	Series HC3
	0.219	1.26	1.33	1.51	1.65	2.2	2.83	Series HMUP3
	0.224	—	—	1.47	1.65	—	—	Series HC1
	0.347	1.10	1.18	1.27	1.4	1.49	1.6	Series HC4
	0.454	1.2	1.25	1.27	1.35	—	1.5	Series HC2
Ovalle and Domingues (1934)[a]	—	—	—	—	—	—	1.59	—
	—	—	—	—	—	—	3.63	With special precautions
Bakhmeteff and Matzke (1936)[b]	—	—	—	—	—	—	2.1	W = 0.152 m
Fawer (1937)	0.1–0.27	—	—	—	1.82	—	2.46	W = 0.303 m
Serre (1953)	—	—	—	—	—	—	1.455	Theory
Binnie and Orkney (1955)	—	—	—	—	—	—	1.74	—
Iwasa (1955)	—	1.5	—	—	—	—	1.9	—
							1.553	Theory
Ryabenko (1990)	0.090	—	—	—	—	—	2.08	Hydrostatic pressure distribution upstream of jump (W = 1 m)
	0.143	—	—	—	—	—	1.90	
	0.147	—	—	—	—	—	1.95	
	0.185	—	—	—	—	—	1.82	
	0.187	—	—	—	—	—	1.86	
	0.192	—	—	—	—	—	1.92	
	0.224	—	—	—	—	—	1.69	
	0.231	—	—	—	—	—	1.77	
	0.239	—	—	—	—	—	1.88	
	0.244	—	—	—	—	—	1.94	
	0.060	—	—	—	—	—	1.01	Nonhydrostatic pressure distribution upstream of jump (W = 1 m)
	0.109	—	—	—	—	—	1.34	
	0.121	—	—	—	—	—	1.02	
	0.010	—	—	—	—	—	1.0	
	0.041	—	—	—	—	—	1.03	
	0.043	—	—	—	—	—	1.25	
	0.044	—	—	—	—	—	1.42	
	0.124	—	—	—	—	—	1.61	

[a]As cited by Montes (1986).

[b]Bakhmeteff and Matzke (1936) indicate an upper limit for undular jumps of F_1 = 1.732, a reanalysis of data indicates the upper limit for their experiments was F_1 = 2.1.

creasing Froude number. Near the disappearance of the undular jump, the length of this region equals one or two wavelengths. For this study, the number of organized (i.e. coherent) wavelengths N_{ow} is best correlated by

$$N_{ow} = \left(15.5 + 3.7\,\frac{y_c}{W}\right)(F^E - F_1) \quad \text{for} \quad F_1 > F^B \tag{6}$$

The writers wish to emphasize that, for a large number of experiments, the damping flow region was clearly observed at the downstream end of the flume. These observations indicate that the chaotic flow region did not result from the reflection of waves by the downstream gate for these experiments. It is believed that the chaotic flow region is a consequence of interactions between the free-surface undulations and the shock waves, when they are not of the same periodicity. In this case, the shock wave propagation disorganizes free-surface undulations and induces a three-dimensional wave motion.

Lateral Shock Waves

When the upstream Froude number nearly equals F^A, weak lateral shock waves develop near the sidewalls, and vanish when they reach the center of the channel (Fig. 7). For Froude numbers larger than F^A, the shock waves extend over the entire width of the channel and are reflected on the opposite sidewall (Fig. 7). The first intersection of the shock waves is always near the top of the first wave crest. Montes (1986) suggested the lateral shock waves (or "Mach" waves) are connected with the existence of the sidewall boundary layers. The sidewall boundary layers retard the fluid near the wall and force the apparition of critical conditions there, sooner than on the channel centerline.

In this study, the appearance of crosswaves is independent of the aspect ratio y_c/W and is around F^A = 1.2 (Table 2). Iwasa (1955) reported observations of lateral waves superposedly on the free-surface undulations for $F_1 \geq 1.5$. Fawer (1937) observed lateral shock waves and presented a photograph of crosswaves.

During the experiments, the centerline flow depth h_* at the start of the crosswaves, and the

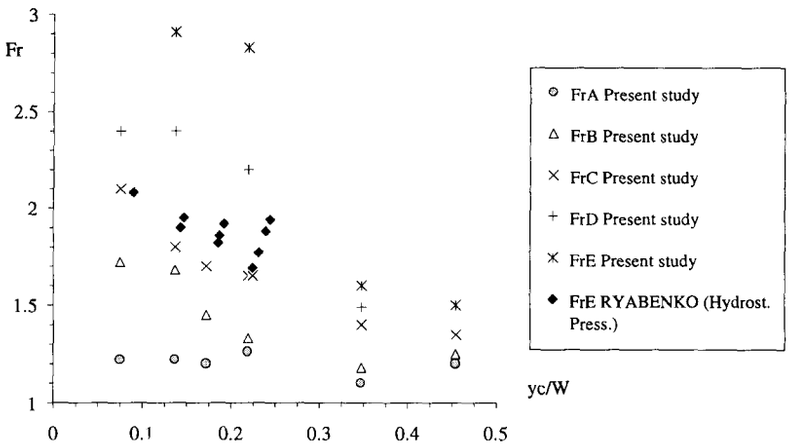

FIG. 5. Characteristic Froude Numbers as Function of Aspect Ratio y_c/W

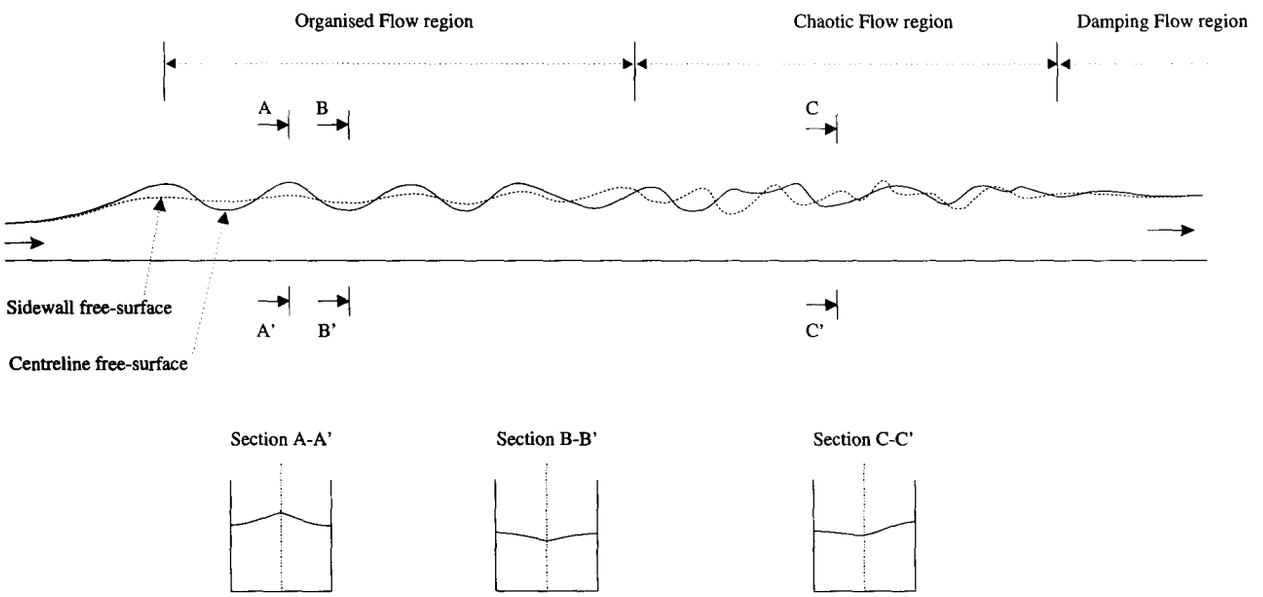

FIG. 6. Flow Regions Downstream of First Crest: Organized, Chaotic, Damping Flow Regions

angle θ_* between the crosswaves and the sidewalls were recorded. The results indicate that the local Froude number $F_* = q_w/\sqrt{g\ h_*^3}$ and θ_* are independent of the aspect ratio y_c/W and functions of the upstream Froude number only. The start of the oblique jump occur in a supercritical flow region such as

$$F_* = F_1 - 0.122 \tag{7}$$

The angle of the shock waves and sidewalls ranges from 20° to 50°, increasing slightly with increasing upstream Froude numbers

$$\theta_* = 33.32\ F_1^{0.232} \tag{8}$$

where θ_* is in degrees, and (7) and (8) are the best fit of the experimental data. Eq. (8) is in opposition with the classical theory of shock waves in supercritical flow (e.g., Rouse 1938; Engelund and Munch-Petersen 1953), which predicts a reduction in the angle θ_* with increasing Froude numbers.

Experimental data and (8) indicate a decrease of the crosswave length, with increasing Froude numbers. But the rate of decrease in length required by the shock waves to cross the flume is much smaller than the rate of decrease of the free-surface wavelength.

The lateral shock waves are a main feature of the undular jump. They appear in a region of positive pressure gradient (i.e., $dP/dx > 0$), in which the modification of the vertical velocity and pressure distributions interacts with lateral (sidewall) boundary layers. The writers believe

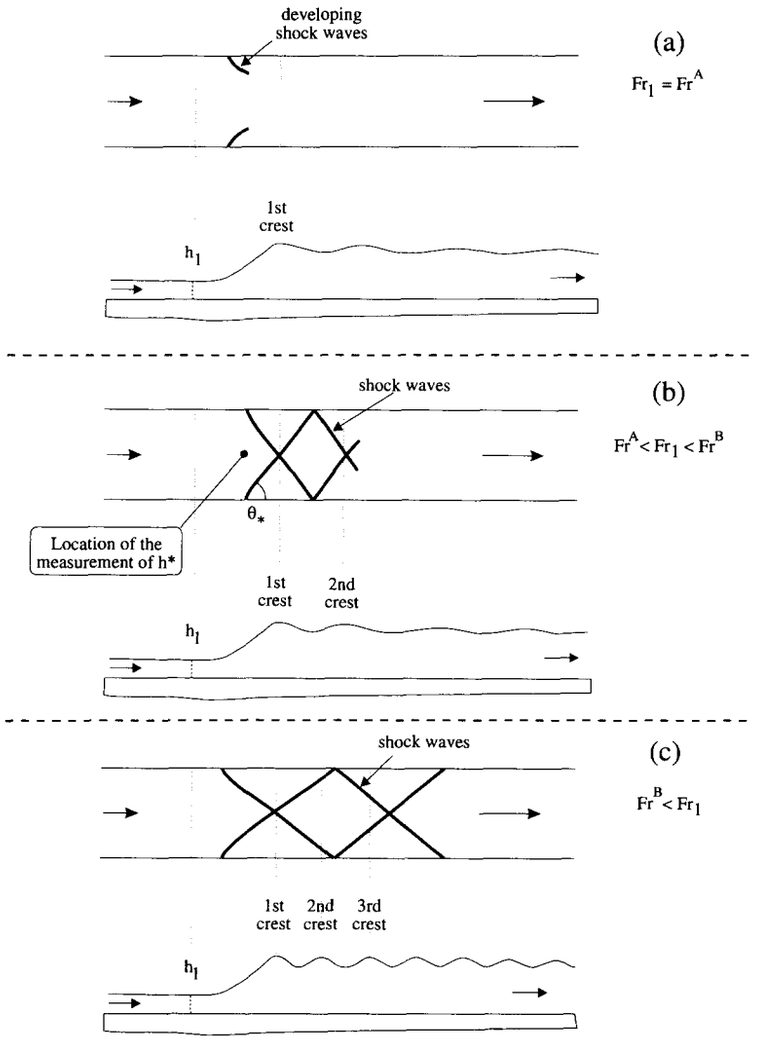

FIG. 7. Lateral Shock Waves (Top View)

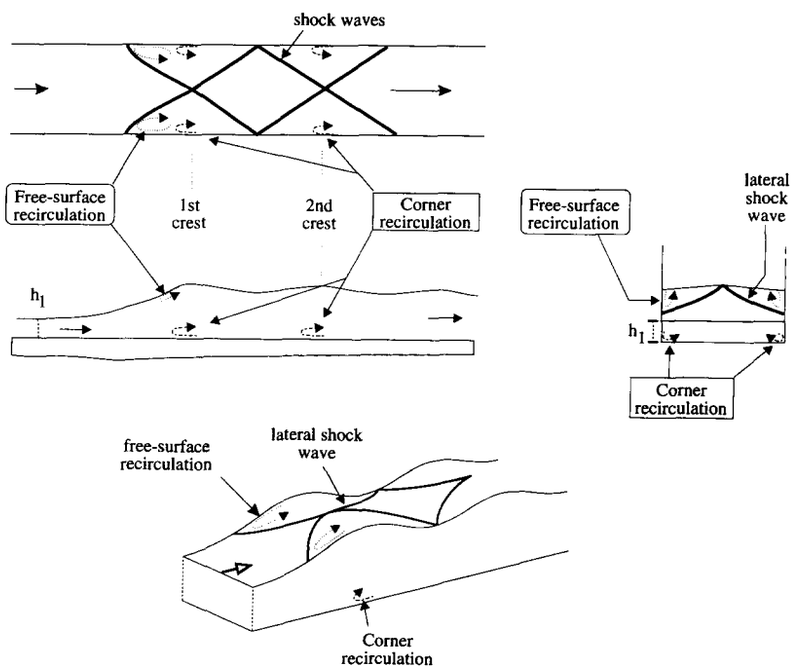

FIG. 8. Recirculatory Flow Motion Near Free Surface and in Corners

that the lateral shock waves result from these interactions. In essence, the wall boundary layer is subjected to a sudden adverse pressure gradient, which causes a sharp deceleration of the velocity near the wall and, possibly, separation. Indeed, a recirculation of the flow indicating separation is observed immediately behind the lateral shock waves near the wall. This is commented upon in the following section. In any case, the complete process is not yet fully understood.

Flow Recirculation

Dye injections were used to observe recirculations or separation bubbles at various locations along undular jumps near the bottom or along the sidewalls. Two types of recirculation are visualized: a free-surface recirculation at the first crest and a corner recirculation at the location of the first crest and sometimes at subsequent crest locations (Fig. 8).

Immediately after the apparition of lateral shock waves (i.e., $F_1 > F^{A1}$), and at the first crest only (Fig. 8), countercurrents are clearly observed near the free surface between the developing shock waves and the sidewalls for jump types *B*, *C*, *D*, and *E* (Fig. 8 shows a type C jump). A large-scale vortex of quasi-vertical axis develops along each sidewall next to the free surface and immediately upstream of the first crest. Visual observations suggest that the strength of the recirculatory motion increases with increasing Froude number for $F_1 > F^{A1}$.

For larger Froude numbers, another form of recirculation becomes apparent near the corners formed by the channel bottom and the sidewalls (Fig. 8). This corner recirculation is located at the first wave crest cross section and at second and successive crest positions for increasing Froude numbers (Table 3). This type of recirculation is not observed elsewhere. At the first wave crest, the corner recirculating motion does not interact with the free-surface recirculation. It is thought that this recirculatory motion is generated by interactions between the expanding flow motion immediately upstream of the wave crest, the sidewall boundary layers, and the bottom boundary layer.

Fawer (1937), Montes (1986), and Yasuda et al. (1993) observed a separation bubble on the bottom centerline of the channel below the first crest. In their experiments, the undular jump was located immediately downstream of a sluice gate and the upstream flow was partially developed. During the present series of experiments, dye injection indicated no recirculation or separation bubble on the centerline next to the channel bottom.

EXPERIMENTAL RESULTS

Free-Surface Profiles

For discharges per unit width ranging from 0.008 to 0.12 m^2/s and upstream Froude numbers between 1.05 and 3.0, the free-surface profiles on the centerline were recorded upstream and downstream of the jump. The complete set of data were reported in Chanson (1993).

Figs. 9 and 10 present the dimensionless wave lengths and wave amplitudes (on the channel centerline) as functions of the upstream Froude number. The data are compared with the solution of the Boussinesq equation developed by Andersen (1978).

Wavelength

For small Froude numbers, the measured wavelengths are close to the solution of the Boussinesq equation (Fig. 9). For larger Froude numbers, the relationship between the dimensionless wavelength and the Froude number is no longer unique, but depends on the ratio of the critical depth over the channel width; i.e., for a given Froude number, the wavelength increases with a decrease in the aspect ratio y_c/W.

One possible explanation is related to the appearance of the surface's lateral shock waves. The writers believe the shock waves affect the wavelength and induce a dependence of the wavelength on the channel width when the free-surface wavelength becomes shorter than the distance along the channel necessary for shock waves to cross the channel (i.e., $F_1 > F^{B}$).

TABLE 3. Onset of Recirculation

Froude number (1)	y_c/W 0.138 (2)	y_c/W 0.217 (3)	Comments (4)
F^{RFS}	1.25	1.26	Apparition of free-surface recirculation.
F^{R1C}	1.41	1.35	Apparition of corner recirculation at first wave crest.
F^{R2C}	1.50	1.47	Apparition of corner recirculation at second wave crest.
F^{R3C}	1.64	1.52	Apparition of corner recirculation at third wave crest.

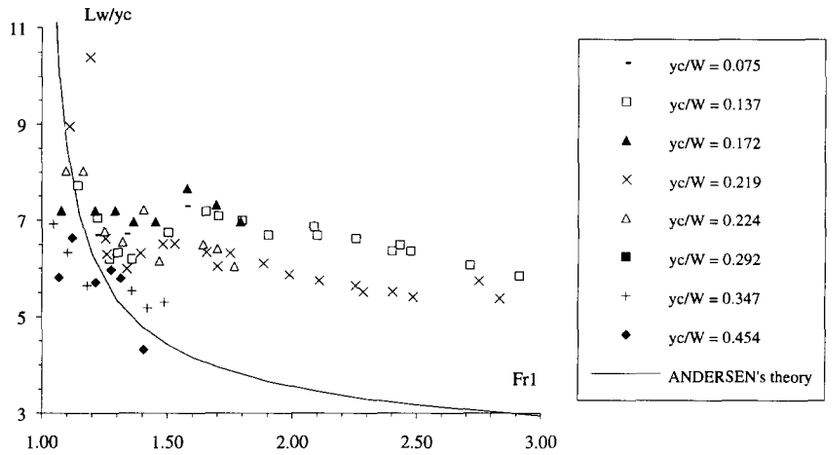

FIG. 9. Dimensionless Wavelength L_w/y_c as Function of Upstream Froude Number F_1

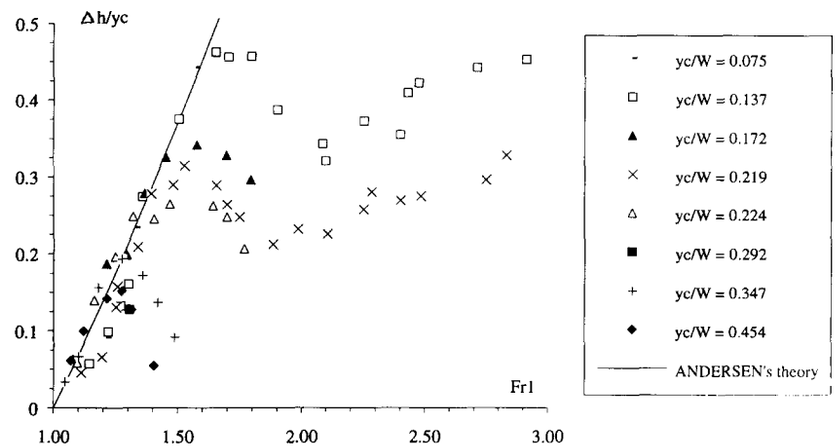

FIG. 10. Dimensionless Wave Amplitude $\Delta h/y_c$ as Function of Upstream Froude Number

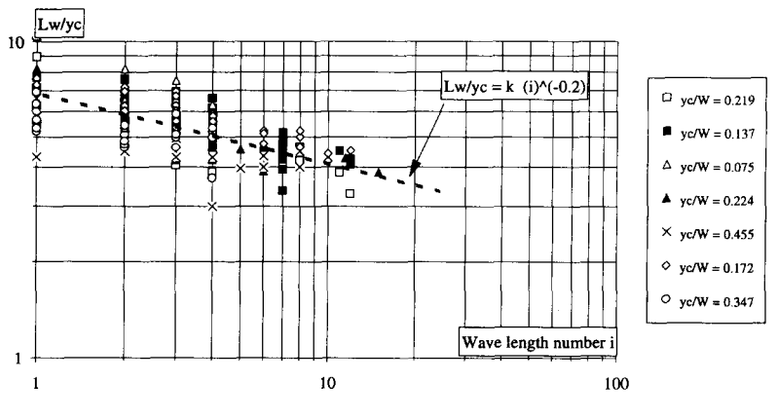

FIG. 11. Dimensionless Wavelength L_w/y_c as Function of Wavelength Number

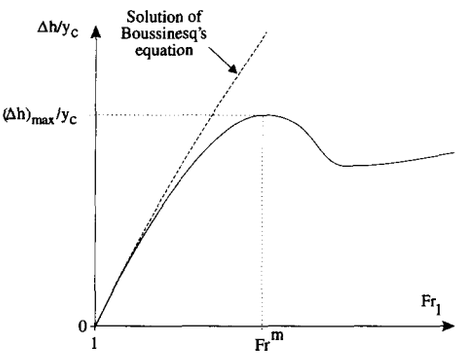

FIG. 12. Dimensionless Wave Amplitude-Upstream Froude Number Relationship (First Wavelength)

For a constant Froude number, a decrease of discharge (and of blockage ratio) gives an increase in the dimensionless wavelength (Fig. 9). For a constant Froude number, a decrease in discharge implies an increase of relative roughness and channel friction. This result is opposite to the findings of Zienkiewicz and Sandover (1957), who studied undular surges and found the channel friction reduced the wavelength. It is thought that the analogy between undular surge and undular jump cannot be applied to this situation.

Fig. 11 shows the dimensionless wavelength as a function of the wavelength number: the ith wavelength is measured between the ith wave crest and the $(i + 1)$-th crest. The analysis of all data clearly indicates that wavelengths decay exponentially along the channel (Fig. 11). Further,

it shows that the rate of decay is independent of the upstream Froude number, of the aspect ratio, and of the type of undular jump. For the experiments, the wavelength decay can be correlated by

$$\frac{L_{wi}}{L_{w1}} = (i)^{-1/5} \tag{9}$$

where L_{w1} = first wavelength; and i = wavelength number (Fig. 11).

Wave Amplitude

Fig. 10 shows that the relationship between the dimensionless wave amplitude and the upstream Froude number has a distinctive shape. The shape is generalized in Fig. 12 and can be described as follow:

1. For Froude numbers close to unity, the data closely follow the theoretical solution of the Boussinesq equation (Andersen 1978). The wave amplitude is almost proportional to the Froude number [i.e., $\Delta h/y_c \propto \mathsf{F}_1 - 1$)].
2. With an increasing Froude number, the wave amplitude data start diverging from the solution of the motion equation (i.e., this equation neglecting energy dissipation considerations) and reach a maximum value $(\Delta h)_{max}$. This trend is consistent with the data presented by both Iwasa (1955) and Montes (1979), and with a reanalysis of the data of Binnie and Orkney (1955).
3. For larger Froude numbers, the wave amplitude decreases with an increasing Froude number.
4. Before the disappearance of free-surface undulations, the wave amplitude stops decreasing with an increasing F_1. At the limit, when the undular jump tends to become a weak jump, the amplitude of the first wave will tend toward a value equal to half of the roller height, and the amplitude of the second wave will tend toward zero (Fig. 10).

Fig. 10 distinctly shows that both the divergence of the data with the Boussinesq equation solution and the maximum dimensionless undulation amplitude are functions of the aspect ratio. For these experiments, the experimental data of the maximum wave amplitude $(\Delta h)_{max}$ and the corresponding upstream Froude number Fr'' (Fig. 12) can be correlated by

$$\frac{(\Delta h)_{max}}{y_c} = 0.0748 \left(\frac{y_c}{W}\right)^{0.894} \quad ; \quad \mathsf{Fr}'' = 1.02 \left(\frac{y_c}{W}\right)^{-0.247} \tag{10, 11}$$

Eqs. (10) and (11) were obtained for $0.137 < y_c/W < 0.454$.

The Froude number Fr'' approximately equals the Froude number F^B, characterizing the appearance of a "cockscomb" roller on the first wave crest (Table 2, columns 4 and 5). It is believed that the wave-breaking mechanism, associated with the small roller, contributes to the reduction of the wave amplitude.

Fawer (1937) was able to set up undular jumps at variable distances downstream of a gate. He noted that the undulations were steeper and more two-dimensional when the jump was close to the gate, i.e., when the upstream boundary layer was thin ($\delta/h_1 << 1$), in which δ is the boundary layer thickness.

Visual observations and measurements show that the longitudinal decay of the wave amplitude is very small, sometimes zero, and a decay of wavelengths along the flume is consistently observed for all experiments. Darcy and Bazin (1865) established an undular jump at the end of a 75-m-long channel, the upstream flow conditions of the jump being fully developed. A reanalysis of their data similarly indicates no decay of wave amplitude along the channel. With regard to partially developed upstream shear flows, Fawer (1937) reported the wave amplitude did not decay along the 5-m-long channel.

Velocity, Pressure, and Specific Energy Distribution on Centerline

For various Froude numbers and discharges, measurements of centerline velocity, pressure, and total head distributions were performed at various locations along the undular jump; i.e., upstream of the jump (*U/S*), at the start of the lateral shock waves (*SW*), at the first crest (1*C*) and first bottom (1*B*), at the second crest (2*C*) and second bottom (2*B*), and at the third crest (3*C*). The complete set of data was presented in Chanson (1993).

Fig. 13 presents a typical set of experimental data obtained along the channel centerline. The pressure distributions (Fig. 13a) are presented as $P/(\rho_w g\, h)_{CL}$ versus y/h, in which P = pressure; and h = centerline flow depth. In Fig. 13b, the dimensionless velocity $V/(V_m)_{CL}$ is plotted as a function of y/h in which V = local velocity; and $(V_m)_{CL}$ = mean centerline velocity

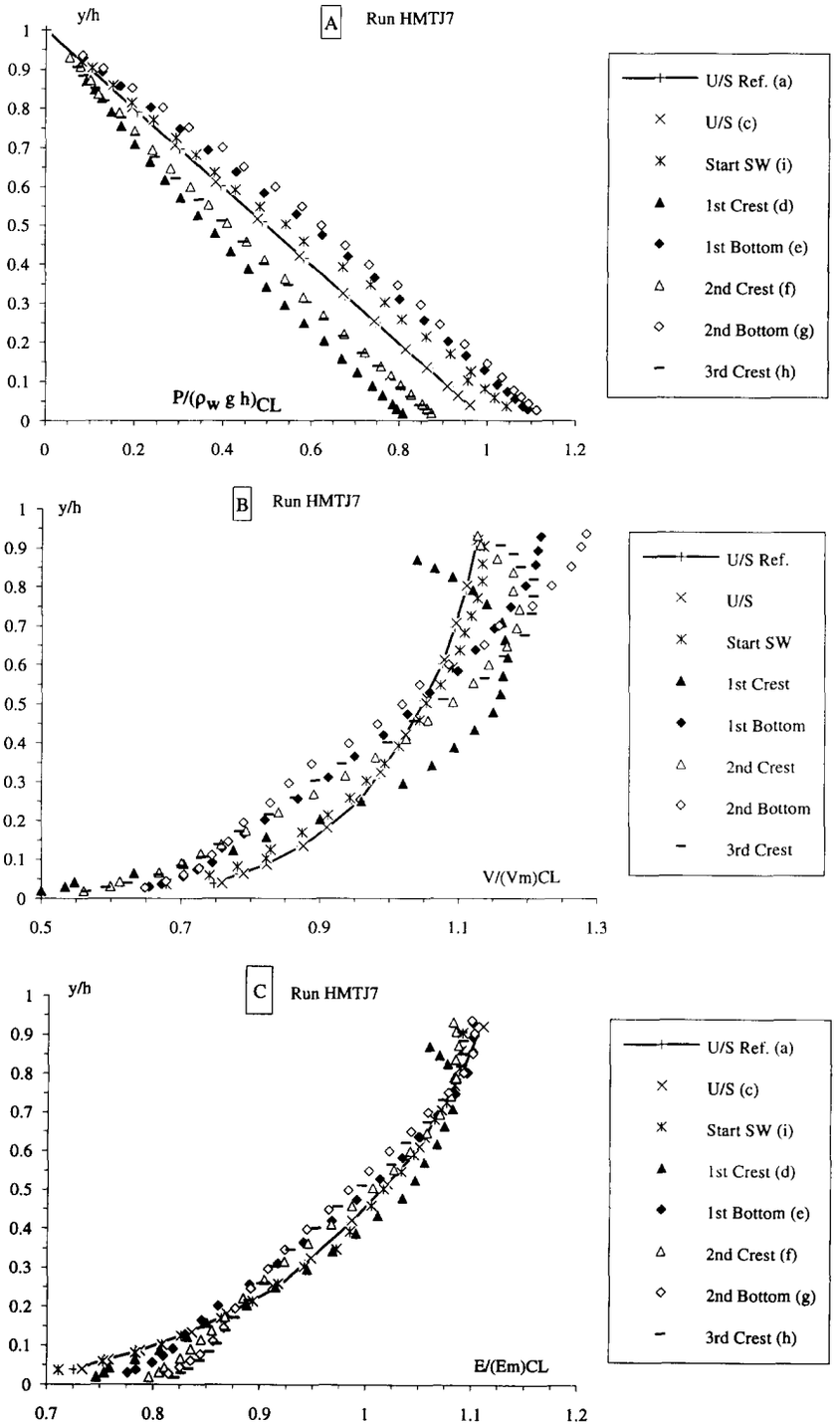

FIG. 13(a). Dimensionless Distributions along Centerline (Undular Jump Type C): Dimensionless Pressure Distributions $P/(\rho_w gh)_{CL}$; (b) Dimensionless Distributions along Centerline (Undular Jump Type C): Dimensionless Velocity Distributions $V/(V_m)_{CL}$; (c) Dimensionless Distributions along Centerline (Undular Jump Type C): Dimensionless Specific Energy Distributions $E/(E_m)_{CL}$

$$(V_m)_{CL} = \left(\frac{1}{h}\int_{y=0}^{y=h} V\,dy\right)_{CL} \tag{12}$$

Fig. 13c shows the dimensionless specific energy $E/(E_m)_{CL}$ as a function of y/h. The local specific energy E = energy per unit weight and gravity unit, with the elevation datum being taken as the bottom of the channel (Chow 1959).

$$E = \frac{P}{\rho_w g} + y\cos\alpha + \frac{V^2}{2g} \tag{13}$$

in which channel slope; and the mean specific energy on the centerline $(E_m)_{CL}$ is defined as:

$$(E_m)_{CL} = \left(\frac{\int_{y=0}^{y=h} EV\, dy}{\int_{y=0}^{y=h} V\, dy} \right)_{CL} \tag{14}$$

Fig. 13a provides a comparison between the pressure distributions along the jump and the upstream hydrostatic pressure distribution (denoted "U/S Ref." in Fig. 13). In Fig. 13b, the velocity distributions can be compared with the upstream power law velocity distribution [(4)].

COMMENT: EFFECTS OF ASPECT RATIO

For open-channel flows, the Froude number equals the ratio of the mean flow velocity over the celerity of small disturbances, and is analogous to the Mach number for compressible flows. As the Mach number for compressible flows, the Froude number is the most important correlating parameter when flow depths are almost critical flow depths; i.e., when the mean specific energy is near its minimum value. In an undular jump, critical flow occurs somewhere between the upstream flow cross section and the first wave crest. At that location (i.e., $h = y_c$), the sidewalls induce a blockage effect that can be best described by the aspect ratio y_c/W. For a wide channel (i.e., two-dimensional flow), the aspect ratio is zero and the sidewalls have no effect on the flow. For a narrow channel (i.e., y_c/W large), the sidewalls induce significant three-dimensional effects.

All the present experiments were performed with a constant channel width and various flow rates. Additional flow visualizations were conducted in a wider channel at the University of Tasmania. Previous experiments were conducted by several authors with various channel widths ranging from 0.2 to 1 m (Table 1).

A reanalysis of all data (i.e., $W = 0.2$ to 1 m) indicates, in each case, a similar dependence of the flow characteristics on the critical depth y_c. The relationship wave amplitude Froude number (Figs. 10 and 12) exhibits similar features for all experiments. Further, a comparison of all experimental results in term of y_c/W shows that, for constant Froude number, the dimensionless wavelength L_w/y_c and amplitude $\Delta h/y_c$ increase with a decreasing aspect ratio y_c/W (Fig. 9 and 10). The upper limit of the undular jump F^E decreases with an increasing y_c/W, for fully developed upstream flow conditions (Table 2 and Fig. 5).

The writers believe the blockage ratio y_c/W is a major parameter, but not the only one characterizing the undular jump. Ryabenko (1990) and Chanson (1993) showed that upstream flow conditions (i.e., partially developed or fully developed boundary layer flow) strongly affect flow characteristics. Further, the characteristics of the sidewall boundary layers are important parameters. For fully developed upstream flows, the writers are convinced that the relative roughness of the sidewall $(k_s)_{wall}/(W/2)$, and hence the channel width, may be a significant parameter. Presently there is no quantitative information on the dependence of flow characteristics on these variables.

CONCLUSION

New undular hydraulic jump experiments were performed in a long tilting flume of rectangular cross section. The upstream flows were fully developed shear flows.

Visual and photographic investigations indicate five different types of undular jumps, the main flow patterns of which are completely different from undular surge flows. The present study shows that the shape of the jump and its main flow characteristics are strongly correlated to the upstream Froude number and aspect ratio y_c/W.

One characteristic feature of undular jumps is the presence of lateral shock waves for Froude numbers larger than 1.2. The shock waves start in a region of supercritical flow and intersect at the first wave crest. The angle θ_* between the shock waves and sidewalls increases with an increasing Froude number. This result contradicts the theory of shock waves, and is not explained yet.

Free-surface profiles were recorded for a wide range of discharge and Froude numbers. For small Froude numbers, the first wavelength and wave amplitude can be estimated by undular surge theory calculations. But for increasing Froude numbers, both the first wavelength and amplitude become dependent on the aspect ratio; i.e., for a given Froude number, the dimensionless first wavelength and amplitude increase with a decreasing ratio y_c/W. Other results of this series of experiments show wave amplitudes as large as $(0.47\ y_c)$, disappearance of the undular jump for upstream Froude numbers ranging from 1.5 to 2.9, an exponential decay of the wavelength along an undular jump, and a small or zero decay of the wave amplitude along the jump.

This paper emphasizes the three-dimensional flow characteristics of undular jumps with fully developed upstream flows in a rectangular channel. Further work is required in the form of

three-dimensional measurements of both free-surface level and velocity, pressure, and total head distributions along these jumps. Additional work is necessary to understand the mechanisms of lateral shock waves.

APPENDIX I. REFERENCES

Andersen, V. M. (1978) "Undular hydraulic jump." *J. Hydr. Engrg.*, ASCE, 104(8), 1185 – 1188.

Bakhmeteff, B. A., and Matzke, A. E. (1936). "The hydraulic jump in terms of dynamic similarity." *Trans.*, ASCE, Vol. 101, 630 – 647.

Binnie, A. M., and Orkney, J. C. (1955). "Experiments on the flow of water from a reservoir through an open channel. II. The formation of hydraulic jump." *Proc., Royal Soc., London*, London, England, Series A, Vol. 230, 237 – 245.

Chandran, K. K., and Venkatraman, C. P. (1985). "Hydraulic design of pump intake for cooling water pumps parli thermal power station (Unit IV), Maharashtra, India." *Proc., Int. Conf. Hydr. of Pumping Stations*, BHRA Publications, Manchester, England, Paper 11, 139 – 148.

Chanson, H. (1993). "Characterstics of undular hydraulic pumps." *Res. Rep. No. CE146*, Dept. of Civ. Engrg., Univ. of Queensland, Australia, (Nov.).

Chen, C. L. (1990). "Unified theory on power laws for flow resistance." *J. Hydr. Engrg.*, ASCE, 117(3), 371 – 389.

Chow, V. T. (1959). *Open channel hydraulics*, McGraw-Hill International, New York, N.Y.

Darcy, H., and Bazin, H. (1865). *Recherches hydrauliques*. Imprimerie Impériales, Parties 1e et 2e, Paris, France (in French).

Engelund, F., and Munch-Petersen, J. (1953). "Steady flow in contracted and expanded rectangular channels: some considerations concerning the shape of the water surface." *Jl La Houille Blanche*, (Aug./Sept.), 464 – 474.

Fawer, C. (1937). "Etude de quelques ecoulements permanents á filets courbes [Study of some steady flows with curved streamlines]," thesis, Lausanne, Switzerland (in French).

Hager, W. H., and Hutter, K. (1984). "On Pseudo-uniform flow in open channel hydraulics." *Acta mechanica*, Vol. 53, 183 – 200.

Haslewood, D. (1985). "Ships in restricted water (Critical Conditions)." *Proc., Inst. Civ. Engrs.*, Part 2, Vol 79, (June), 275 – 293.

Henderson, F. M. (1966). *Open channel flow*. MacMillan Co., New York, N.Y.

Isaacs, L. T., and Macintosh, J. C. (1988). "Boundary shear stress measurement in open channels." *Res. Rep. No. CE85*, Dept. of Civ. Engrg., Univ. of Queensland, Brisbane, Australia.

Iwasa, Y. (1955). "Undular jump and its limiting conditions for existence." *Proc., 5th Japan Nat. Congr. for Appl. Mech., Paper II-14*, Japan, 315 – 319.

Jones, L. E. (1964). "Some observations on the undular jump." *J. Hydr. Engrg.*, ASCE, 90(3), 69 – 82.

Lemoine, R. (1948). "Sur les Ondes Positives de Translation dans les Canaux et sur le Ressaut Ondulé de Faible Amplitude." *J. La Houille Blanche*, (Mar. – Apr.), 183 – 185 (in French).

Montes, J. S. (1979). "Undular hydraulic jump — discussion." *J. Hydr. Engrg.*, ASCE, 105(9), 1208 – 1211.

Montes, J. S. (1986). "A study of the undular jump profile." *Proc., 9th Australasian Fluid Mech. Conf.*, AFMC, Auckland, New Zealand, 148 – 151.

Ovalle, A., and Dominguez, A. (1934). "Civil engineering," thesis, Catholic Univ., Santiago, Chile.

Rouse, H. (1938). *Fluid mechanics for hydraulic engineers*. McGraw-Hill, New York, N.Y.

Ryabenko, A. A. (1990). "Conditions favorable to the existence of an undulating jump *Gidrotekhnicheskoe Stroitel'stvo*, No. 12, 29–34 (in Russian). (Translated in Hydrotechnical Const., 1990, Plenum Publ., 762 – 770).

Sandover, J. A., and Holmes, P. (1962). "The hydraulic jump in trapezoidal channels." *Water Power*, (Nov.), 445 – 449.

Serre, F. (1953). "Contribution á l'Etude des Ecoulements Permanents et Variables dans les Canaux." *Jl La Houille Blanche*, (Dec.), 830 – 872 (in French).

Streeter, V. L., and Wylie, E. B. (1981). *Fluid mechanics*, 1st Ed., McGraw-Hill, New York, N.Y.

Yasuda, Y., Ohtsu, I., and Gotoh, H. (1993). "A few experiments on undular hydraulic jump." *48th Annu. Meeting*, Japan Soc. of Civ. Engrg. (JSCE), Tokyo, Japan, Sept., II – 159 (in Japanese).

Zienkiewicz, O. C., and Sandover, J. A. (1957). "The undular surge wave." *Proc., 7th IAHR Congress*, Vol. II, IAHR, Lisbon, Portugal, D1 – 11.

APPENDIX II. NOTATION

The following symbols are used in this paper:

h = flow depth (m) measured perpendicular to channel bottom;
y_c = critical flow depth (m) for rectangular channel $y_c = \sqrt[3]{q_w^2/g}$;
h_* = centerline flow depth (m) at start of lateral shock waves;
E = specific energy (m);
$(E_m)_{CL}$ = mean specific energy (m) on centerline;
F = Froude number defined as $\mathsf{F} = q_w/\sqrt{g\,h^3}$;
F^A = Froude number characterizing apparition of lateral shock waves;
F^B = Froude number characterizing apparition of small "cockscomb" roller at top of first wave crest;
F^C = Froude number characterizing apparition of individual air bubble entrainment;
F^D = Froude number characterizing apparition of roller formed between lateral shock waves and substantial air entrainment;
F^E = Froude number characterizing disappearance of undular jump;
F^m = upstream Froude number corresponding to maximum wave amplitude;

F^{RFS} = Froude number characterizing onset of free-surface recirculation at first crest;
F^{R1C} = Froude number characterizing onset of corner recirculation at first crest;
F^{R2C} = Froude number characterizing onset of corner recirculation at second crest;
F^{R3C} = Froude number characterizing onset of corner recirculation at third crest;
F_* = Froude number defined in term of centerline flow depth at inception of lateral shock waves: $F_* = q_w\sqrt{g/h_*^3}$;
f = Darcy friction factor;
g = gravity constant $g = 9.80$ m/s^2 in Brisbane, Australia;
H = total head (m);
i = wavelength number;
K = Von Karman constant;
k = constant of proportionality;
k_s = equivalent sand roughness height (m);
L_w = wavelength (m);
N = exponent of power law velocity distribution;
N_{ow} = number of organized wavelengths;
P = pressure (Pa);
Q_w = water discharge (m^3/s);
q_w = water discharge per unit width (m^2/s);
V = velocity (m/s);
V_c = critical flow velocity (m/s); $V_c = q_w/y_c$;
V_{max} = maximum velocity on centerline (m/s) (at free surface);
$(V_m)_{CL}$ = mean velocity on centerline (m/s);
W = channel width (m);
x = distance along channel bottom (m);
y = distance measured perpendicular to channel bottom (m);
z = bed elevation (m) taken positive upward;
α = channel slope;
ΔH = head loss (m);
Δh = wave amplitude (m);
$(\Delta h)_{max}$ = maximum wave amplitude (m);
δ = boundary layer thickness (m);
θ_* = angle between lateral shock waves and sidewalls at start of lateral shock waves;
ρ_w = water density (kg/m^3); and
$\emptyset$ = diameter (m).

Subscript

CL = on flume centerline;
i = wavelength number;
1 = flow conditions upstream of hydraulic jump; and
2 = flow conditions downstream of hydraulic jump.